university of groningen

University Medical Center Groningen

University of Groningen

The solar photospheric abundance of carbon

Caffau, E.; Ludwig, H.-G.; Bonifacio, P.; Faraggiana, R.; Steffen, M.; Freytag, B.; Kamp, I.; Ayres, T. R.

Published in:
Astronomy & astrophysics

DOI:
10.1051/0004-6361/200912227

IMPORTANT NOTE: You are advised to consult the publisher's version (publisher's PDF) if you wish to cite from it. Please check the document version below.

Document Version
Publisher's PDF, also known as Version of record

Publication date:
2010

Link to publication in University of Groningen/UMCG research database

Citation for published version (APA):
Caffau, E., Ludwig, H-G., Bonifacio, P., Faraggiana, R., Steffen, M., Freytag, B., Kamp, I., & Ayres, T. R. (2010). The solar photospheric abundance of carbon: Analysis of atomic carbon lines with the CO5BOLD solar model. *Astronomy & astrophysics*, *514*, [A92]. https://doi.org/10.1051/0004-6361/200912227

Copyright
Other than for strictly personal use, it is not permitted to download or to forward/distribute the text or part of it without the consent of the author(s) and/or copyright holder(s), unless the work is under an open content license (like Creative Commons).

The publication may also be distributed here under the terms of Article 25fa of the Dutch Copyright Act, indicated by the “Taverne” license. More information can be found on the University of Groningen website: https://www.rug.nl/library/open-access/self-archiving-pure/taverne-amendment.

Take-down policy
If you believe that this document breaches copyright please contact us providing details, and we will remove access to the work immediately and investigate your claim.

Downloaded from the University of Groningen/UMCG research database (Pure): http://www.rug.nl/research/portal. For technical reasons the number of authors shown on this cover page is limited to 10 maximum.

Download date: 05-05-2023

A&A 514, A92 (2010)
DOI: 10.1051/0004-6361/200912227
© ESO 2010

Astronomy & Astrophysics

The solar photospheric abundance of carbon

Analysis of atomic carbon lines with the CO5BOLD solar model

E. Caffau[1], H.-G. Ludwig[2,1,3], P. Bonifacio[2,1,4], R. Faraggiana[5], M. Steffen[6], B. Freytag[7], I. Kamp[8], and T. R. Ayres[9]

[1] GEPI, Observatoire de Paris, CNRS, Université Paris Diderot, 92195 Meudon Cedex, France
e-mail: Elisabetta.Caffau@obspm.fr
[2] CIFIST Marie Curie Excellence Team
[3] Zentrum für Astronomie der Universität Heidelberg, Landessternwarte, Königstuhl 12, 69117 Heidelberg, Germany
[4] Istituto Nazionale di Astrofisica, Osservatorio Astronomico di Trieste, via G.B. Tiepolo 11, 34143 Trieste, Italy
[5] Università degli Studi di Trieste, via G.B. Tiepolo 11, 34143 Trieste, Italy
[6] Astrophysikalisches Institut Potsdam, An der Sternwarte 16, 14482 Potsdam, Germany
[7] CRAL,UMR 5574: CNRS, Université de Lyon, École Normale Supérieure de Lyon, 46 allée d'Italie, 69364 Lyon Cedex 7, France
[8] Kapteyn Astronomical Institute, Postbus 800, 9700 AV Groningen, The Netherlands
[9] Center for Astrophysics and Space Astronomy, University of Colorado 389 UCB (CASA), Boulder, CO 80309-0389, USA

Received 29 March 2009 / Accepted 9 February 2010

ABSTRACT

Context. The analysis of the solar spectra using hydrodynamical simulations, with a specific selection of lines, atomic data, and method for computing deviations from local thermodynamical equilibrium, has led to a downward revision of the solar metallicity, Z. We are using the latest simulations computed with the CO5BOLD code to reassess the solar chemical composition. Our previous analyses of the key elements, oxygen and nitrogen, have not confirmed any extreme downward revision of Z, as derived in other works based on hydrodynamical models.
Aims. We determine the solar photospheric carbon abundance with a radiation-hydrodynamical CO5BOLD model and compute the departures from local thermodynamical equilibrium by using the Kiel code.
Methods. We measured equivalent widths of atomic C I lines on high-resolution, high signal-to-noise ratio solar atlases of disc-centre intensity and integrated disc flux. These equivalent widths were analysed with our latest solar 3D hydrodynamical simulation computed with CO5BOLD. Deviations from local thermodynamic equilibrium we computed in 1D with the Kiel code, using the average temperature structure of the hydrodynamical simulation as a background model.
Results. Our recommended value for the solar carbon abundance relies on 98 independent measurements of observed lines and is $A(\mathrm{C}) = 8.50 \pm 0.06$. The quoted error is the sum of statistical and systematic errors. Combined with our recent results for the solar oxygen and nitrogen abundances, this implies a solar metallicity of $Z = 0.0154$ and $Z/X = 0.0211$.
Conclusions. Our analysis implies a solar carbon abundance that is about 0.1 dex higher than what was found in previous analyses based on different 3D hydrodynamical computations. The difference is partly driven by our equivalent width measurements (we measure, on average, larger equivalent widths than the other work based on a 3D model), in part because of the different properties of the hydrodynamical simulations and the spectrum synthesis code. The solar metallicity we obtain from the CO5BOLD analyses is in slightly better agreement with the constraints of helioseismology than the previous 3D abundance results.

Key words. Sun: abundances – stars: abundances – hydrodynamics – line: formation

1. Introduction

The importance of an accurate knowledge of the solar abundances can hardly be overstated since they serve as the reference for all other celestial objects. The good performance of the new-generation instruments allows accurate stellar abundances to be derived and therefore the requested accuracy of the reference solar abundances is increased. This can, at least partly, explain the current revival in spectroscopic solar abundance studies. The very large gap in resolution between solar and stellar spectra, which existed until a few decades ago, is diminishing rapidly. The majority of recent solar abundance determinations relies on observational data that are almost 30 years old, both for the disc-centre intensity and for the integrated disc flux (Jungfraujoch grating spectra and Kitt Peak Fourier Transform Spectra, respectively).

For a long time, solar abundances were considered as well established, and only minor refinements were suggested by each new study, usually driven by improved atomic or molecular data. By using atomic or molecular lines, or both, the many analyses of the photospheric solar carbon made in 1980–2000, were converging toward the value of $A(\mathrm{C}) = 8.52 \pm 0.06$ (Grevesse & Sauval 1998), which was slightly lowering the previous values by including the appropriate NLTE corrections. However, Allende Prieto et al. (2002) have announced a large downward revision of the C abundance from the analysis of the forbidden [CI] 872.7 nm line ($A(\mathrm{C}) = 8.39 \pm 0.04$). A subsequent paper by Asplund et al. (2005a) also obtained a similar downward revision of the carbon abundance when using permitted atomic and molecular lines.

The new abundances of C, as well as those of other elements, conflict with some solar properties; for instance, solar models

(Yang & Bi 2007) and helioseimology (Basu & Antia 2008; Chaplin & Basu 2008; Delahaye & Pinsonneault 2006) cannot be reconciled with the recent revision of solar abundances by Asplund et al. (2005b). Solar abundances of the light elements, which have the highest cosmic abundance, are particularly important for understanding stellar and galactic composition. Besides being the main contributors to the solar metallicity Z, the CNO abundances are useful for studying the depletion in the interstellar gas (ISM). For example, the comparison of the C/O ratio in the ISM with that in the solar photosphere tells us how much C has been locked into dust. Also studying the diffusion effects in the corona and solar wind requires using photospheric solar abundances as a reference. Because it is a highly volatile element, carbon has partly escaped carbonaceous chondrites, so that the solar system abundance of C mainly relies on the analysis of the photospheric spectrum.

The solar spectrum is rich in atomic C lines, as well as in lines of C-bearing molecules. Because of its high first ionisation potential (11.26 eV), the measurable lines of carbon in the Sun are only those of C I. Several tens of C I lines are present in the visual and near IR spectrum, but only a few are suitable for abundance analysis. The chosen lines should be weak, unblended, with accurately known transition probabilities and, ideally, formed in LTE. Strong lines, with large equivalent width (EW hereafter, $EW \geq 15-20$ pm) should be rejected because the collisional damping constants are uncertain. Only one forbidden line, at 872.7126 nm, has been detected in the solar spectrum.

Molecular lines are highly temperature sensitive and require very accurate analysis of the photospheric thermal structure as the one made by Ayres et al. (2006) for the infrared CO features. Holweger (2001) prefers to consider only atomic lines, while Grevesse et al. (1987) derive the carbon abundance from the vibration-rotation and pure rotation lines of the CO and CN diatomic molecules.

In the present paper we analyse only C I atomic transitions to derive the solar photospheric carbon abundance.

Table 1. Lines considered for the abundance determination.

λ nm	Quality	λ nm	Quality
477.000	3	1165.968	3
477.5907	2	1174.822	2
505.2167	1	1177.754	1
538.0336	1	1180.110	3
658.7608	2	1184.873	1
708.5511	3	1186.299	1
708.7827	2	1189.291	1
711.1475	2	1189.575	1
711.3180	1	1254.948	2
713.2112	3	1256.212	1
783.7105	2	1256.904	1
801.8564	1	1258.159	1
833.5149	1	1261.410	3
872.7126	2	1602.164	3
875.3079	3	1704.516	3
887.3390	3	1723.448	3
906.1432	1	1734.638	2
907.8278	1	1744.860	1
911.1797	1	1745.597	1
918.2831	3	1747.591	3
960.3032	2	1750.564	1
962.0795	3	1755.446	3
965.8435	1	1763.738	2
1012.3871	1	1778.960	2
1054.1241	2	2102.313	2
1068.5345	1	2121.155	2
1070.7333	1	2125.989	2
1072.9533	1	2290.656	2
1075.3985	1	3085.462	3
1161.929	3	3129.748	2
1163.050	3	3406.579	3
1165.884	3	3991.177	3

Notes. Quality: 1 good line, 2 line with problems, 3 line rejected.

2. Selection of lines

As a starting point, we looked at a sample obtained by combining the C I lines chosen by Grevesse et al. (1991), Bièmont et al. (1993), Takeda (1994), and Asplund et al. (2005a) (see Table 1). We examined these lines, comparing the available solar atlases among them and to synthetic profiles. We excluded from our analysis those lines that we judged too heavily blended (e.g. the line at 477.0 nm) compared to the synthetic spectra or the lines for which the disagreement among observed spectra was unexplained and too large (e.g. the line at 1180.1 nm). Furthermore, we eliminated the lines whenever we suspected a significant contamination from telluric absorption, based on the comparison of the observed atlases and synthetic spectra, and also on the inspection of spectra of rapidly rotating stars, indicating the presence of telluric lines (e.g. the line at 1602.1 nm). The excluded lines are flagged by "3" in the columns "Quality" of Table 1. The final list of our sample of lines, labelled as Quality "1" or "2" in Table 1, is given in Table 3. We labelled as "1" those lines that are not blended, or the blends are negligible in comparison to the C I line, or we think we are able to model the blends. We labelled as "2" the lines we are less confident in. These lines show differences among the observed spectra (e.g. the line at 711.1 nm) or we can hardly reproduce their shape with a synthetic profile (e.g. the line at 1734.6 nm) or we are not confident of being able to take the telluric absorptions into account (e.g. the line at 1778.9 nm). The final selection consists of 45 individual lines for which we have 98 EW measurements. The subsample of good data, labelled "Quality = 1", contains 25 lines, 66 measured EWs.

For the abundance determination, one could rely on line-profile fitting or on EW measurements. The line-profile fitting procedure has many advantages because not only the strength of the line is taken into account, but also the line shape. When the synthetic line profile provides a faithful reproduction of the line shape, we consider this procedure superior. We stress here that by "line-profile" fitting we mean fitting with a synthetic profile, computed by using all the known lines in the range. But "fitting" with a synthetic profile consisting of a single line is conceptually identical to measuring the EW by fitting with a Gaussian or Voigt profile, although it has the advantage of correctly treating the line asymmetry, which is, however, in general irrelevant for abundance work. If poorly known blends interfere, the EW measurement procedure with deblending (see below) is the more reliable option. The present analysis is based on EW measurements. We prefer this approach because of the following problems with the available C I lines.

– A large fraction of the lines are blended and the atomic data of the contaminants are not well known, so that, when included in the 3D synthetic spectra, the comparison with the observed spectra is not reliable. Measurement of the EW, on the other hand, can be reliable, since the extra absorption can be modelled by a suitable Gaussian or Voigt profile.

– Some of the lines are contaminated by telluric absorption; also in this case, the contaminating telluric absorption can be modelled as above providing a reliable measure of the *EW*.
– The continuum placement is problematic for some lines, because of neighbouring lines whose atomic data are often poorly known. The *EW* measurement with `splot`, on the other hand, is designed to handle such situations.
– NLTE effects, not taken into account in the 3D synthetic profile, can change the shape of the line.

The last point has not yet been investigated in detail since no 3D-NLTE analysis for carbon is available at the moment. But we expect that carbon does not behave differently from oxygen, and it is shown in Asplund et al. (2004) that the 3D-NLTE line profile is different from the 3D-LTE one. One could consider using the line-profile fitting technique for clean lines, which form a small subsample of the complete set of lines, reserving the *EW* measurement to the "problematic" lines. However, in this way the analysis would not be homogeneous over the complete sample of lines. The adopted method of *EW* measurements also allows a more direct comparison with other analyses in the literature.

For measuring the *EW* we used the IRAF[1] (Tody 1993) task `splot`. In the case of blended lines, we used the deblending option of `splot`, which permits fitting the spectral profile with a number of Gaussian and/or Voigt functions. In this way any known line in a range can be simulated with a theoretical profile. Generally for weak lines we used a Gaussian profile to fit the observed profile, while we used a Voigt function for strong lines. For unblended lines we also used direct integration. We are aware that the observed profile is asymmetric, while both Gaussian and Voigt functions are symmetric. Several experiments convinced us that the use of a Voigt profile to measure the *EW* of an asymmetric 3D profile provides a measurement of the *EW* which differs from the real one by less than 1%. This error is surely negligible when compared to the uncertainty of the *EW* measurement due to the continuum placement, which in the case of a typical observed spectrum can reach 5%.

For the majority of the lines, the *EW*s we obtain are close to the values of Bièmont et al. (1993), but not for all. We could compare only the Delbouille disc-centre spectrum, which is the observed data considered in Bièmont et al. (1993). In principle, strong lines should be rejected because of uncertain values of NLTE corrections and line broadening parameters that become important. We keep these strong lines anyway in the sample, because they do not disagree with the other lines, and there is no evident trend for the abundance as a function of the *EW*.

When available, we used $\log gf$ from NIST (Wiese et al. 1996), as retrieved from the ASD database (Ralchenko 2005). The values are given in Table 3. All $\log gf$-values used in Bièmont et al. (1993), except the one of the 801.8 nm line, are very close to the values of NIST. For our sample of C I, lines the NIST database relies on four sources (Luo & Pradhan 1989; Hibbert et al. 1993; Nussbaumer & Storey 1984; Weiss 1996), the main one being Hibbert et al. (1993), which covers all the lines.

For the Van der Waals broadening constants, we proceeded as in Caffau et al. (2008). When available (for 35 lines of our sample), we relied on Barklem et al. (1998) values. For the remaining lines, we used the WIDTH approximation, implemented in the Kurucz routine WIDTH (see Ryan 1998). If we remove the lines without Van der Waals broadening constants from Barklem et al. (1998), the derived carbon abundance is less than 0.03 dex higher than when considering the complete sample of lines. Therefore we decided to keep all the lines we selected for the abundance determination.

[1] IRAF is distributed by the National Optical Astronomy Observatories, which are operated by the Association of Universities for Research in Astronomy, Inc., under cooperative agreement with the National Science Foundation.

Table 2. Comparison of the disc-centre *EW* of two C I lines determined by different authors.

λ (nm)	*EW* (pm)			
	G91	B93	A05	C10
960.30	10.8	9.62	9.6	11.5
2102.31	10.0	10.26	8.76	10.0

Notes. G91: Grevesse et al. (1991), B93: Bièmont et al. (1993), A05: Asplund et al. (2005a), and C10: this work.

3. Equivalent widths in the literature

Reliable observed *EW*s are those measured by Grevesse et al. (1991) and by Bièmont et al. (1993) on the disc-centre Jungfraujoch Atlas. The values used by Stürenburg & Holweger (1990) are taken from the *EW* measurements by Baschek & Holweger (1967), which were based on old atlases, and the ones in Asplund et al. (2005a) are the *EW*s of the synthetic best-fit profile. Only two lines have been considered in all four analyses, and they are presented in Table 2.

For the line at 960.3036 nm, we find a significantly larger *EW* than the three other authors, whose results agree closely. On the other hand, our *EW* for the line at 2102.3151 nm is very similar to those by Grevesse et al. (1991) and Bièmont et al. (1993), while the theoretical *EW* derived by Asplund et al. (2005a) from their 3D model by using their best-fit abundance is much lower (see Table 2), even though the measured *EW*s should be corrected for blending.

We note that Bièmont et al. (1993) gave a low weight to both of these lines, presumably because they are affected by telluric absorption and other blends, making reliable *EW*s difficult to measure. Nevertheless, Table 2 demonstrates once again that *EW* measurements differ considerably from author to author and are a major source of uncertainty.

All the investigations of the solar carbon abundance cited above rely on a single solar atlas. In fact, as already mentioned in Caffau et al. (2008), the available solar atlases do not always agree. This could be due to telluric absorption, to variability in solar spectrum, or to systematic effects related to the different observations. The present analysis is based on four different solar spectra so should yield more reliable abundances.

4. Observed spectra

We considered the same four observed solar atlases that are publicly available that we already used in Caffau et al. (2008). For disc-centre, this is the double-pass grating spectrum taken at Jungfraujoch by Delbouille et al. (1973), ranging from 300 to 1000 nm, and the infrared FTS spectrum taken at Kitt Peak by Delbouille et al. (1981), covering the wavelength range 1000 to 5400 nm (together called Delbouille intensity, DI). In addition, the disc-centre FTS spectrum published by Neckel & Labs (1984) is used (330 to 1250 nm, Neckel intensity, NI). Neckel & Labs (1984); Neckel (1999) also provide a corresponding FTS spectrum for the integrated disc flux (Neckel flux, NF). Another set of Kitt Peak FTS scans by Brault and Testerman has been

Table 3. Line parameters, 3D and 1D carbon abundance (LTE), and 1D NLTE corrections for our sample of selected C I lines.

λ	SP	χ	EW	$\log gf$	Acc.	A(C) (LTE)			3D corrections		1D-NLTE corrections		
nm		eV	pm			3D	⟨3D⟩	$1D_{LHD}$	3D-⟨3D⟩	3D-$1D_{LHD}$	1.0	1/3	0.0
872.7126	DI	1.26	0.47	−8.140	B	8.428	8.401	8.388	0.027	0.040	0.000	0.000	0.000
872.7126	NI	1.26	0.47	−8.140	B	8.426	8.399	8.386	0.027	0.040	0.000	0.000	0.000
872.7126	KF	1.26	0.46	−8.140	B	8.382	8.360	8.354	0.021	0.028	0.000	0.000	0.000
872.7126	NF	1.26	0.47	−8.140	B	8.390	8.369	8.362	0.021	0.028	0.000	0.000	0.000
477.5907	DI	7.49	1.71	−2.304	C	8.698	8.709	8.709	−0.011	−0.011	−0.003	−0.007	−0.017
477.5907	NI	7.49	1.75	−2.304	C	8.711	8.722	8.721	−0.011	−0.010	−0.003	−0.007	−0.017
477.5907	KF	7.49	1.42	−2.304	C	8.687	8.716	8.697	−0.029	−0.010	−0.006	−0.013	−0.030
477.5907	NF	7.49	1.43	−2.304	C	8.691	8.720	8.701	−0.029	−0.010	−0.006	−0.013	−0.030
505.2167	DI	7.68	4.04	−1.303	B	8.428	8.429	8.402	−0.000	0.026	−0.007	−0.015	−0.036
505.2167	NI	7.68	4.15	−1.303	B	8.449	8.449	8.422	0.000	0.028	−0.007	−0.015	−0.036
505.2167	KF	7.68	3.56	−1.303	B	8.456	8.482	8.442	−0.026	0.014	−0.013	−0.026	−0.065
505.2167	NF	7.68	3.54	−1.303	B	8.452	8.478	8.438	−0.026	0.014	−0.013	−0.026	−0.065
538.0336	DI	7.68	2.55	−1.616	B	8.444	8.447	8.428	−0.004	0.016	−0.007	−0.014	−0.034
538.0336	NI	7.68	2.53	−1.616	B	8.439	8.442	8.423	−0.004	0.016	−0.007	−0.014	−0.034
538.0336	KF	7.68	2.19	−1.616	B	8.465	8.490	8.458	−0.025	0.007	−0.012	−0.025	−0.060
538.0336	NF	7.68	2.20	−1.616	B	8.468	8.492	8.461	−0.025	0.007	−0.012	−0.025	−0.060
658.7608	DI	8.54	1.65	−1.003	B	8.316	8.322	8.293	−0.006	0.023	−0.004	−0.009	−0.018
658.7608	NI	8.54	1.68	−1.003	B	8.326	8.332	8.303	−0.006	0.023	−0.004	−0.009	−0.018
658.7608	KF	8.54	1.34	−1.003	B	8.343	8.369	8.336	−0.026	0.007	−0.007	−0.016	−0.030
658.7608	NF	8.54	1.33	−1.003	B	8.339	8.365	8.332	−0.026	0.007	−0.007	−0.016	−0.030
708.7827	DI	8.65	0.72	−1.442	C	8.413	8.423	8.401	−0.010	0.012	−0.004	−0.008	−0.017
711.1475	DI	8.64	1.30	−1.085	B	8.348	8.355	8.328	−0.006	0.021	−0.004	−0.009	−0.020
711.3180	DI	8.65	2.73	−0.773	B	8.468	8.467	8.430	0.001	0.039	−0.005	−0.011	−0.026
711.3180	NI	8.65	2.75	−0.773	B	8.473	8.472	8.434	0.001	0.039	−0.005	−0.011	−0.026
711.3180	KF	8.65	2.45	−0.773	B	8.563	8.582	8.544	−0.019	0.018	−0.009	−0.020	−0.045
711.3180	NF	8.65	2.39	−0.773	B	8.547	8.566	8.529	−0.019	0.018	−0.009	−0.020	−0.045
783.7105	DI	8.85	0.22	−1.778	B	8.363	8.373	8.353	−0.010	0.010	−0.003	−0.006	−0.012
801.8564	DI	8.85	0.13	−2.130	D	8.480	8.489	8.470	−0.009	0.010	−0.002	−0.005	−0.011
833.5149	DI	7.68	12.30	−0.437	B+	8.606	8.570	8.508	0.037	0.098	−0.069	−0.121	−0.225
833.5149	NI	7.68	12.70	−0.437	B+	8.642	8.605	8.542	0.037	0.100	−0.069	−0.121	−0.225
833.5149	KF	7.68	10.70	−0.437	B+	8.661	8.646	8.602	0.014	0.058	−0.108	−0.185	−0.318
833.5149	NF	7.68	10.60	−0.437	B+	8.650	8.636	8.592	0.014	0.058	−0.108	−0.185	−0.318
906.1432	DI	7.48	16.50	−0.347	B	8.643	8.597	8.532	0.045	0.111	−0.074	−0.127	−0.236
907.8278	DI	7.48	13.50	−0.581	B	8.640	8.597	8.536	0.043	0.104	−0.059	−0.104	−0.201
911.1797	DI	7.49	17.50	−0.297	B	8.665	8.620	8.553	0.045	0.112	−0.054	−0.109	−0.223
911.1797	NI	7.49	17.70	−0.297	B	8.678	8.633	8.566	0.045	0.112	−0.054	−0.109	−0.223
911.1797	KF	7.49	15.20	−0.297	B	8.715	8.690	8.642	0.025	0.074	−0.146	−0.231	−0.384
911.1797	NF	7.49	15.50	−0.297	B	8.739	8.714	8.664	0.025	0.075	−0.146	−0.231	−0.384
960.3032	DI	7.48	11.50	−0.896	B	8.727	8.686	8.630	0.041	0.098	−0.039	−0.073	−0.130
965.8435	DI	7.49	17.00	−0.280	B	8.559	8.512	8.447	0.047	0.112	−0.042	−0.094	−0.179
1012.3871	DI	8.54	11.80	−0.031	C+	8.682	8.651	8.589	0.031	0.094	−0.032	−0.063	−0.118
1012.3871	NI	8.54	11.60	−0.031	C+	8.665	8.634	8.572	0.031	0.093	−0.032	−0.063	−0.118
1012.3871	KF	8.54	9.41	−0.031	C+	8.677	8.672	8.626	0.006	0.051	−0.056	−0.106	−0.170
1012.3871	NF	8.54	9.35	−0.031	C+	8.671	8.665	8.620	0.006	0.051	−0.056	−0.106	−0.170
1054.1241	DI	8.54	2.03	−1.398	D	8.728	8.725	8.699	0.004	0.030	−0.009	−0.017	−0.042
1054.1241	NI	8.54	1.95	−1.398	D	8.706	8.703	8.677	0.003	0.029	−0.009	−0.017	−0.042
1054.1241	KF	8.54	1.75	−1.398	D	8.800	8.814	8.788	−0.014	0.011	−0.016	−0.032	−0.074
1054.1241	NF	8.54	1.65	−1.398	D	8.767	8.781	8.756	−0.015	0.010	−0.016	−0.032	−0.074
1068.5345	DI	7.48	20.20	−0.272	B	8.605	8.556	8.489	0.050	0.116	−0.067	−0.117	−0.205
1068.5345	NI	7.48	20.00	−0.272	B	8.594	8.544	8.478	0.050	0.116	−0.067	−0.117	−0.205
1068.5345	KF	7.48	17.80	−0.272	B	8.668	8.640	8.588	0.028	0.080	−0.107	−0.188	−0.340
1068.5345	NF	7.48	17.50	−0.272	B	8.648	8.620	8.569	0.028	0.080	−0.107	−0.188	−0.340
1070.7333	DI	7.48	18.50	−0.411	B	8.638	8.589	8.524	0.050	0.114	−0.047	−0.090	−0.193
1070.7333	NI	7.48	18.20	−0.411	B	8.619	8.570	8.505	0.050	0.114	−0.047	−0.090	−0.193
1070.7333	KF	7.48	16.80	−0.411	B	8.735	8.707	8.656	0.028	0.078	−0.127	−0.207	−0.357
1070.7333	NF	7.48	16.00	−0.411	B	8.678	8.651	8.601	0.027	0.077	−0.127	−0.207	−0.357
1072.9533	DI	7.49	18.20	−0.420	B	8.644	8.594	8.529	0.050	0.115	−0.040	−0.089	−0.190
1072.9533	NI	7.49	17.80	−0.420	B	8.618	8.568	8.504	0.050	0.115	−0.040	−0.089	−0.190
1072.9533	KF	7.49	15.80	−0.420	B	8.687	8.660	8.611	0.028	0.077	−0.120	−0.199	−0.342
1072.9533	NF	7.49	15.60	−0.420	B	8.672	8.645	8.596	0.027	0.076	−0.120	−0.199	−0.342
1075.3985	DI	7.49	4.54	−1.606	B	8.489	8.467	8.435	0.022	0.055	−0.012	−0.025	−0.055
1075.3985	NI	7.49	4.48	−1.606	B	8.480	8.458	8.426	0.022	0.054	−0.012	−0.025	−0.055
1075.3985	KF	7.49	3.64	−1.606	B	8.477	8.478	8.454	−0.001	0.023	−0.023	−0.045	−0.095

Table 3. continued.

λ	SP	χ	EW	$\log gf$	Acc.	A(C) (LTE)			3D corrections		1D-NLTE corrections		
nm		eV	pm			3D	$\langle$3D$\rangle$	$1D_{LHD}$	3D-$\langle$3D$\rangle$	3D-$1D_{LHD}$	1.0	1/3	0.0
1075.3985	NF	7.49	3.61	−1.606	B	8.471	8.472	8.449	−0.001	0.023	−0.023	−0.045	−0.095
1174.8220	DI	8.64	14.90	0.375	B	8.368	8.330	8.267	0.038	0.102	−0.029	−0.060	−0.138
1174.8220	NI	8.64	14.80	0.375	B	8.362	8.323	8.260	0.038	0.101	−0.029	−0.060	−0.138
1174.8220	NF	8.64	12.40	0.375	B	8.392	8.381	8.327	0.011	0.064	−0.032	−0.086	−0.211
1177.7540	DI	8.64	6.56	−0.520	B	8.514	8.488	8.443	0.026	0.071	−0.015	−0.030	−0.073
1177.7540	NI	8.64	6.58	−0.520	B	8.517	8.491	8.446	0.026	0.071	−0.015	−0.030	−0.073
1177.7540	KF	8.64	5.09	−0.520	B	8.491	8.492	8.455	−0.002	0.036	−0.026	−0.053	−0.125
1177.7540	NF	8.64	5.09	−0.520	B	8.491	8.492	8.455	−0.002	0.036	−0.026	−0.053	−0.125
1184.8730	DI	8.64	5.70	−0.697	B	8.510	8.490	8.452	0.020	0.058	−0.012	−0.025	−0.060
1184.8730	NI	8.64	5.75	−0.697	B	8.516	8.496	8.458	0.020	0.058	−0.012	−0.025	−0.060
1184.8730	KF	8.64	4.66	−0.697	B	8.534	8.538	8.502	−0.004	0.032	−0.023	−0.049	−0.108
1186.2990	DI	8.64	5.81	−0.710	B	8.535	8.514	8.476	0.020	0.059	−0.011	−0.025	−0.061
1186.2990	NI	8.64	5.79	−0.710	B	8.532	8.512	8.474	0.020	0.058	−0.011	−0.025	−0.061
1186.2990	KF	8.64	4.63	−0.710	B	8.541	8.544	8.508	−0.004	0.032	−0.023	−0.049	−0.107
1189.2910	DI	8.64	10.10	−0.277	B	8.518	8.491	8.439	0.027	0.079	−0.020	−0.042	−0.097
1189.2910	NI	8.64	10.10	−0.277	B	8.518	8.491	8.439	0.027	0.079	−0.020	−0.042	−0.097
1189.2910	NF	8.64	8.45	−0.277	B	8.555	8.553	8.506	0.002	0.048	−0.037	−0.076	−0.157
1189.5750	DI	8.65	13.94	−0.008	B	8.530	8.499	8.441	0.031	0.089	−0.027	−0.052	−0.117
1189.5750	NI	8.65	13.97	−0.008	B	8.532	8.501	8.442	0.031	0.090	−0.027	−0.052	−0.117
1189.5750	NF	8.65	11.45	−0.008	B	8.550	8.545	8.492	0.005	0.058	−0.023	−0.073	−0.169
1254.9480	DI	8.85	6.80	−0.565	B	8.632	8.604	8.563	0.028	0.069	−0.008	−0.017	−0.045
1256.2120	DI	8.85	6.89	−0.522	B	8.597	8.569	8.528	0.028	0.069	−0.008	−0.018	−0.047
1256.9040	DI	8.85	5.75	−0.598	B	8.535	8.510	8.473	0.025	0.062	−0.008	−0.017	−0.044
1258.1590	DI	8.85	6.00	−0.536	B	8.502	8.477	8.439	0.026	0.063	−0.008	−0.018	−0.042
1734.6381	DI	9.70	0.64	−1.348	C	8.352	8.336	8.351	0.016	0.001	0.000	0.000	0.003
1744.8600	DI	9.00	21.60	0.012	B+	8.428	8.393	8.359	0.035	0.069	−0.006	−0.015	−0.058
1745.5971	DI	9.70	17.40	0.280	C	8.567	8.534	8.502	0.033	0.066	0.001	0.002	0.008
1750.5641	DI	9.70	17.50	0.424	C	8.430	8.396	8.364	0.034	0.066	0.001	0.001	0.008
1763.7381	DI	9.71	21.00	0.338	C	8.673	8.639	8.600	0.035	0.073	0.001	0.002	0.013
1778.9600	DI	7.95	1.40	−2.246	B	8.247	8.225	8.239	0.022	0.009	−0.003	−0.006	−0.008
2102.3131	DI	9.17	10.00	−0.450 [b]	–	8.651	8.618	8.580	0.033	0.071	−0.001	−0.002	−0.009
2121.1551	DI	9.83	8.56	−0.080 [b]	–	8.660	8.632	8.599	0.027	0.061	0.000	0.000	0.004
2125.9891	DI	9.83	17.80	0.490 [b]	–	8.598	8.566	8.513	0.033	0.085	0.000	0.000	0.004
3129.7480	DI	9.69	2.60	−0.570 [b]	–	8.688	8.673	8.650	0.015	0.039	0.000	0.001	0.002
2290.6561	DI	9.17	12.15	−0.182 [a]	–	8.793	8.763	8.720	0.030	0.073	−0.001	−0.003	−0.013

Notes. $\log gf$-values with their quality (column six) are taken from the NIST database; the quality (Acc.) represents the accuracy of the value, ranging from B+, meaning $\frac{\sigma f}{f} \leq 7\%$, to D, meaning $\frac{\sigma f}{f} \leq 50\%$. $\log gf$ with flag b are from Bièmont et al. (1993), those with flag a are from Asplund et al. (2005a) (no quality is indicated in these cases).

made available by Kurucz (2005a) (300 to 1000 nm, hereafter Kurucz flux, KF). For one line we resorted to the ATMOS solar atlas (Farmer et al. 1989; Farmer 1994).

5. Model atmospheres

We used the same radiation-hydrodynamical model, computed with the CO5BOLD code (Freytag et al. 2002, 2003; Wedemeyer et al. 2004) used in our previous solar abundance analyses. Details of the model can be found in Caffau & Ludwig (2007); Caffau et al. (2008). The same holds for the employed 1D models. As a reference model we used a plane parallel 1D model ($1D_{LHD}$ with mixing-length parameter of 1.0) that shares the micro-physics and radiation transfer scheme with CO5BOLD. We also used a 1D model obtained by temporal and horizontal averaging of the 3D hydrodynamic structure on surfaces of equal optical depth ($\langle$3D$\rangle$), as well as the Holweger-Müller semi-empirical model (Holweger 1967; Holweger & Müller 1974). When necessary, this was put on a column mass scale, assuming the same abundances and opacities as in the CO5BOLD model. For the spectrum synthesis based on the 1D models, we adopted a microturbulence of 1.0 km s^{-1}, both for disc-centre (intensity) and integrated disc (flux) spectra.

6. Results

6.1. The [CI] line at 872.7 nm

There is only one observable forbidden [CI] line, located at 872.7126 nm ($2p^2\ ^1D_2 - 2p^2\ ^1S_0$), with a lower level excitation potential of 1.264 eV. This line is important, because it is weak and therefore insensitive to the assumption about the damping constant and, according to Stürenburg & Holweger (1990), not affected by NLTE.

We measured the EW on the two disc-centre and two integrated disc solar spectra. The result is EW(DI) = 0.511 pm, EW(NI) = 0.509 pm, EW(NF) = 0.517 pm, EW(KF) = 0.508 pm. We subtracted the contribution of the Fe I blending line (λ = 872.7132 nm, $\log gf = -3.93$, χ = 4.186 eV, EW(Int) = 0.040 pm, EW(Flux) = 0.045 pm) according to the 3D computation. The [CI] is formed in LTE, so that the LTE abundance derived from the four observed solar atlases should closely agree. While the two disc-centre and the two integrated disc spectra are in very good agreement with each other, we find

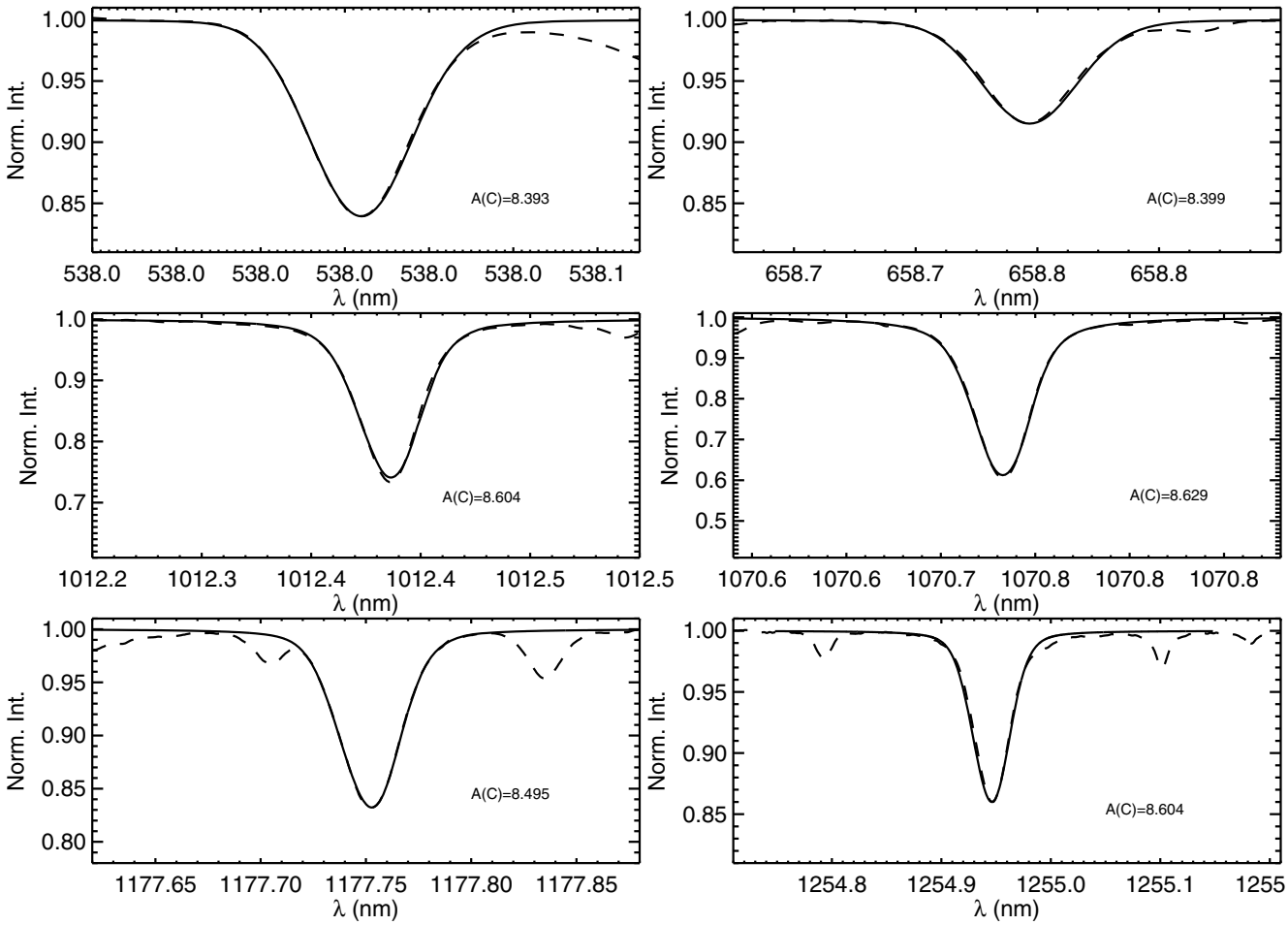

Fig. 1. Comparison of the observed disc-centre solar spectrum (dashed lines, DI for the two reddest lines and NI for the others) with the corresponding 3D synthetic profiles (solid lines) for a selection of clean C I lines.

a difference in the carbon abundance of 0.04 dex between disc-centre and integrated disc spectra. This effect could be attributed to NLTE effects on the blending iron line, which can be different for disc-centre and integrated disc spectra.

6.2. Permitted lines

The abundances derived from all the lines of our sample are assembled in Table 3. Atomic data for each line, the measured *EW*s, and the derived LTE abundances using the 3D, ⟨3D⟩, and $1D_{LHD}$ models are provided in the table. The total 3D correction, defined as 3D-$1D_{LHD}$ is positive for all the lines, except for the 477.5907 nm line. The so-called granulation correction, quantified by the difference 3D-⟨3D⟩ measures the effect of the horizontal temperature fluctuations. It is never very large and may be in the same direction as the total 3D correction, or in the opposite direction, depending on the line. All our permitted C I lines originate in highly excited lower levels ($\chi > 7$ eV). The 3D-⟨3D⟩ corrections for the weaker lines ($EW < 4.0$ pm) in the optical and near infra-red range (450 nm $< \lambda <$ 820 nm) are small and mostly negative (3D-⟨3D⟩ < 0.01). We can compare these 3D-⟨3D⟩ corrections to the value Δ_{gran} defined in Steffen & Holweger (2002). The hydro-simulation they consider is a 2D model, while the 1D model is the temporal and horizontal average over surfaces of equal optical depth of their 2D model, meaning that it is similar to our ⟨3D⟩ model. The C I lines investigated in Steffen & Holweger (2002) have $\lambda = 550$ nm and $EW \approx 0.5$ pm. For $\chi > 6$ eV, Δ_{gran} is indeed slightly negative, (see their Table 1 and their Fig. 5) in qualitative agreement with the results found for comparable C I lines in the present study.

Both 3D corrections (3D-$1D_{LHD}$ and 3D-⟨3D⟩) increase with *EW*, possibly indicating an inadequate choice of the microturbulence parameter for the 1D models. We cannot discern any trend with the excitation energy or the wavelength.

We do not yet have the capability of computing the deviations from local thermodynamic equilibrium (NLTE effects) in the 3D spectrum synthesis, and, to our knowledge, such calculations have not yet been performed elsewhere. As a first approximation, we have therefore computed 1D NLTE corrections using the ⟨3D⟩ model as a background model. For each line we computed NLTE corrections with the Kiel code (Steenbock & Holweger 1984) and the model-atom of Stürenburg & Holweger (1990). The line blanketing is treated with an opacity distribution function as provided by Castelli & Kurucz (2003), assuming solar metallicity and a microturbulence of 2 km s^{-1} . We considered three possible choices for the parameter S_H quantifying the thermalizing effect of collisions with neutral hydrogen according to the generalised Drawin approximation (Drawin 1969) as proposed by Steenbock & Holweger (1984):

1. classical scaling ($S_H = 1$),
2. no effect of collisions with neutral H ($S_H = 0$),
3. intermediate collisional efficiency ($S_H = 1/3$).

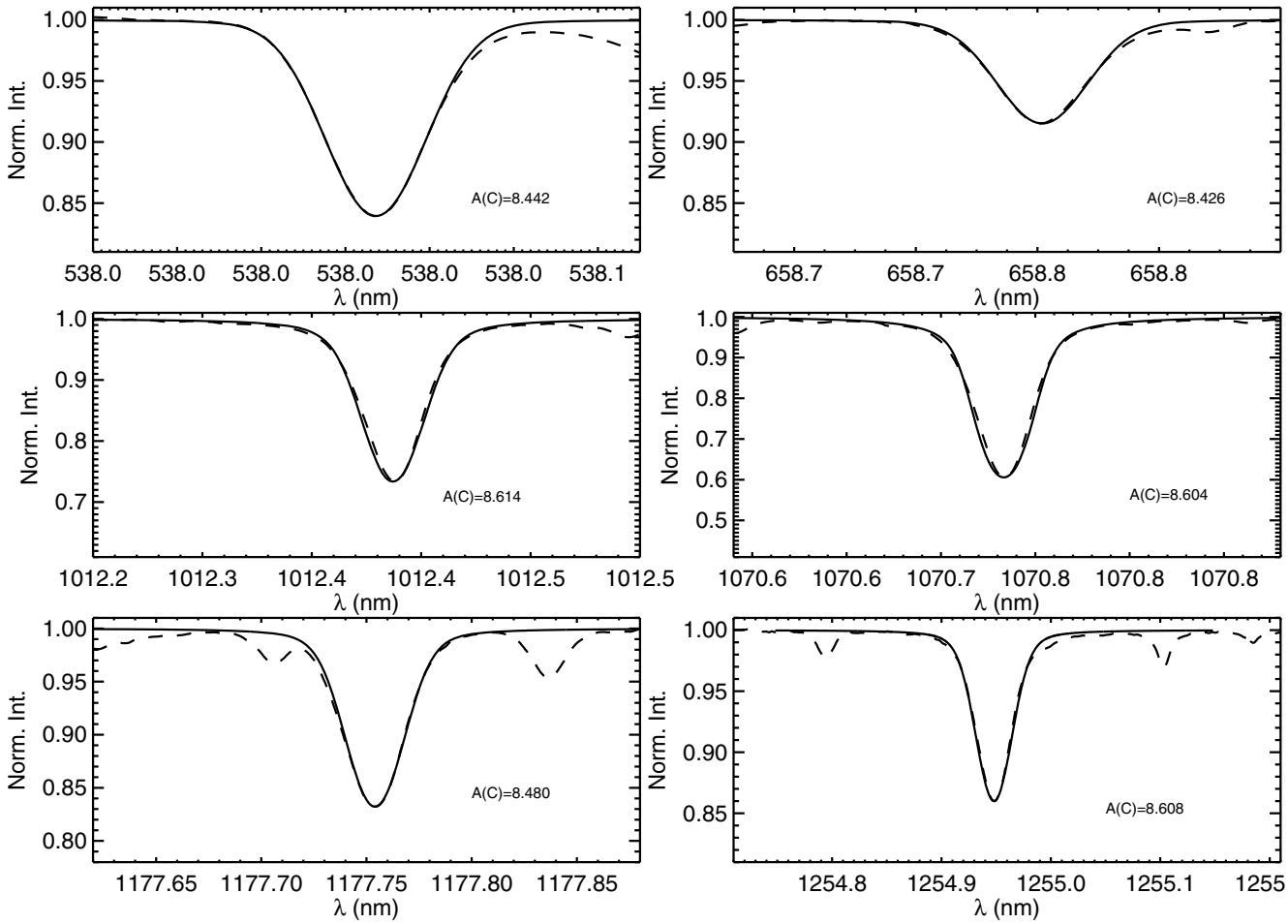

Fig. 2. As Fig. 1, but showing the HM synthetic profile (solid lines) superimposed on the observed solar spectrum (dashed lines). To be consistent with Fig. 1, the synthetic profile is computed with Linfor3D, ignoring any blending lines.

The NLTE correction obtained for each line is listed in Table 3. There is generally good agreement with the NLTE computations of Stürenburg & Holweger (1990) and Asplund et al. (2005a), with a maximum difference of 0.02 dex. We recall that these studies rely on a different model atmosphere for the NLTE computation, so that differences of a few hundredth of dex can easily be attributed to the different input solar model. This agreement in the 1D-NLTE computations is encouraging. As long as no 3D-NLTE computation is available, it is certainly justified to apply this 1D-NLTE correction to our 3D-LTE abundances, as also done by Asplund et al. (2005a) in their careful work.

As explained above, we rely on *EW* measurements for the carbon abundance determination, because a considerable fraction of the lines is blended, and NLTE effects are non-negligible. Nevertheless, it is useful to compare the observed spectrum with the 3D synthetic profiles for some of the cleanest lines. A few examples are shown in Fig. 1. The agreement is encouraging, but the abundance needed to achieve the best (visual) agreement between 3D-synthetic and observed line profile is not always identical to the abundance obtained from matching the *EW*s. This can stem from remaining blends not included in the 3D-synthetic profile, NLTE effects that can change the shape of the line profile, or the adopted damping constants. Comparison of Figs. 1 and 2 shows that the 3D synthetic profiles generally can reproduce the observed profiles of the selected clean C I lines somewhat better than the 1D synthetic profiles calculated from the HM model with a microturbulence of 1.0 km s^{-1} .

6.3. The solar carbon abundance

The final carbon abundance depends only weakly on the assumption made about $S_{\rm H}$. By applying the NLTE corrections to the 3D LTE results and computing the average of the abundances of Table 3, we obtain

$$\begin{array}{llll} A({\rm C}) = & 8.446 \pm 0.121 & \text{for} & S_{\rm H} = 0 \\ A({\rm C}) = & 8.498 \pm 0.110 & \text{for} & S_{\rm H} = 1/3 \\ A({\rm C}) = & 8.523 \pm 0.112 & \text{for} & S_{\rm H} = 1. \end{array} \quad (1)$$

For reference, the results for the HM model are

$$\begin{array}{llll} A({\rm C}) = & 8.449 \pm 0.135 & \text{for} & S_{\rm H} = 0 \\ A({\rm C}) = & 8.503 \pm 0.116 & \text{for} & S_{\rm H} = 1/3 \\ A({\rm C}) = & 8.532 \pm 0.112 & \text{for} & S_{\rm H} = 1. \end{array} \quad (2)$$

The results from CO^{5}BOLD and HM models are in very good agreement. The carbon abundances from the various lines as a function of wavelength are shown in Fig. 3 for the CO^{5}BOLD model and in Fig. 4 for the HM model.

Our favoured value is $A({\rm C}) = 8.498 \pm 0.110$, obtained by applying the NLTE correction, with $S_{\rm H} = 1/3$, to the 3D-LTE abundance. If we restrict the abundance determination to the lines labelled as "Quality=1" in Table 1, the result is $A({\rm C}) = 8.490 \pm 0.048$. The carbon abundance from the subsample is very close to the one obtained from the complete sample, only 0.008 dex smaller, while the line-to-line scatter is much reduced. Nevertheless, we prefer the result from the complete sample,

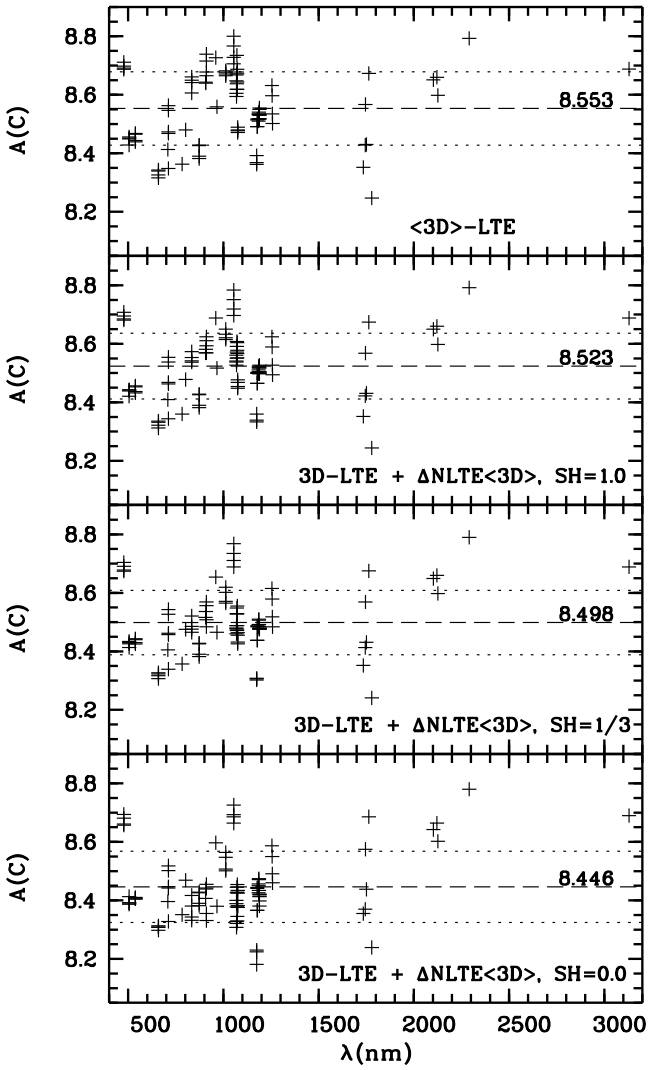

Fig. 3. The carbon abundance as a function of wavelength of the individual C I lines compiled in Table 3, as obtained from the 3D solar model for different assumptions about the 1D NLTE corrections, which are all based on the ⟨3D⟩ model.

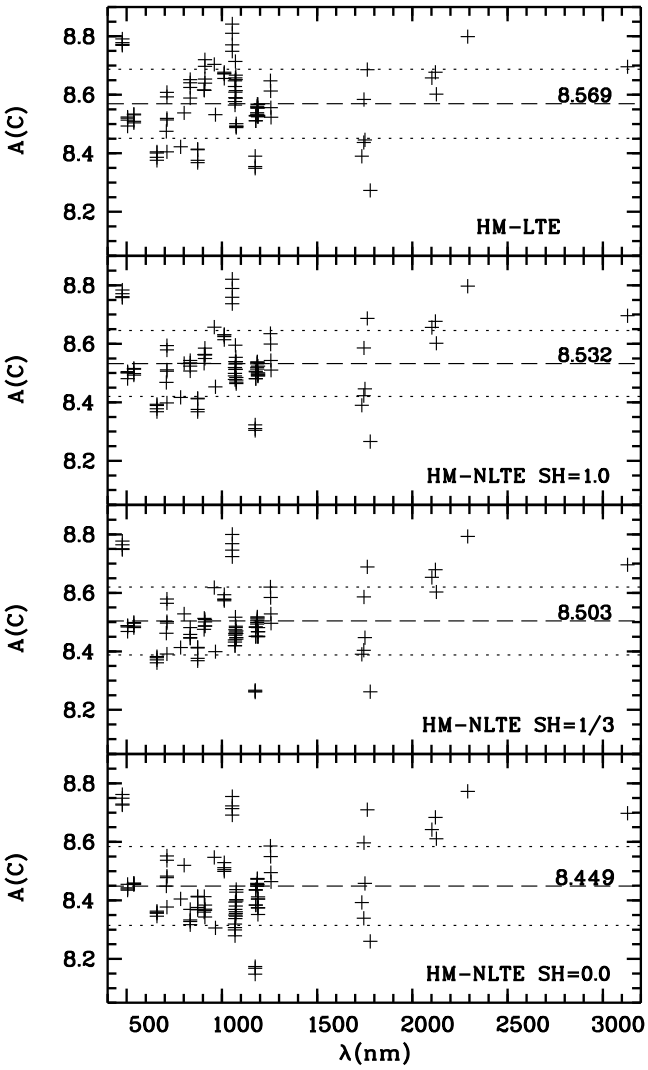

Fig. 4. As Fig. 3, but showing the carbon abundances obtained from the HM model.

since we are aware that the selection of "good" lines is somehow subjective, and hardly changes the mean carbon abundance.

7. Discussion

If we consider the *EW*s of 55 lines in Bièmont et al. (1993), based on Delbouille disc-centre spectra, together with the $\log gf$-values used in that work, we find $A(\mathrm{C}) = 8.518 \pm 0.137$ from our 3D model. If we instead use the updated $\log gf$-values from the NIST database, we obtain $A(\mathrm{C}) = 8.504 \pm 0.125$. This value can be compared to our LTE result, based on the 40 lines in common with Bièmont et al. (1993) and measured in the same solar atlas, of $A(\mathrm{C}) = 8.535 \pm 0.121$ obtained with the 3D model, and of $A(\mathrm{C}) = 8.550 \pm 0.108$ obtained with the HM model. The LTE abundance based on our complete sample of 98 lines is $A(\mathrm{C}) = 8.553 \pm 0.125$ from the 3D model and $A(\mathrm{C}) = 8.569 \pm 0.118$ from the HM model. Our abundance is slightly higher than the one of Bièmont et al. (1993) because of the line selection and differences in the *EW*s for some lines, but the overall agreement is very satisfactory.

The 3D-NLTE abundances are obtained by applying the 1D-NLTE corrections with $S_{\mathrm{H}} = 1/3$ to the individual 3D-LTE abundances. All 98 3D-NLTE abundances lie within 3σ of the mean value, $A(\mathrm{C}) = 8.498 \pm 0.110$. When keeping only abundances within 2σ of the mean value, 94 values meet the cut-off, and the average becomes $A(\mathrm{C}) = 8.492 \pm 0.098$; within 1σ, 70 values still survive, and $A(\mathrm{C}) = 8.485 \pm 0.049$. As expected, the standard deviation becomes smaller, but the average almost remains the same.

To check the validity of the *EW* approach, we used line-profile fitting to determine the carbon abundance for two lines that are not blended, are weak, and that have a very small NLTE correction: 538.0 nm and 658.7 nm. On average, the result is about 0.02 dex below the one obtained from the *EW*. For the majority of the selected lines, the atomic data of the blending components are not very well known. These blending components are, however, separated enough that *EW*s can be measured by fitting multiple Gaussian or Voigt profiles. We therefore prefer to use *EW*s rather than line-profile fitting (see Sect. 2).

We find no obvious trend in the abundance with the lower level energy, neither for the LTE nor for the NLTE results. However, this is not surprising since all carbon lines of our sample originate in similar high excitation levels, since the range in energy is little more than 2 eV.

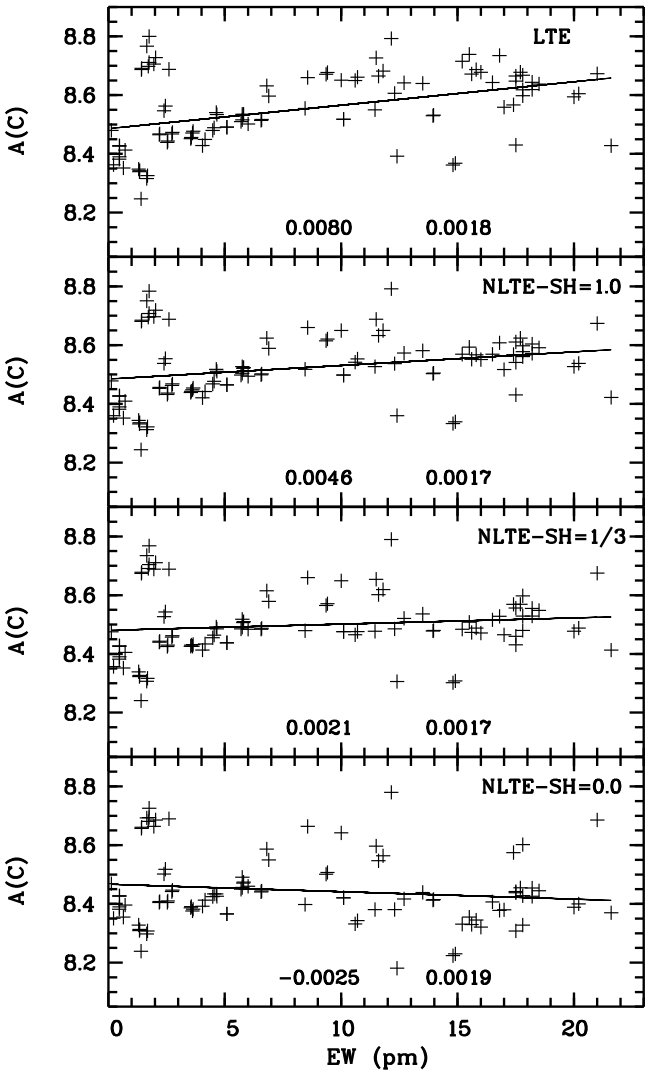

Fig. 5. The carbon abundances as a function of *EW* for the 3D model. The two numbers in the lower part of the plots indicate the slope of the best-fit linear relation and its 1σ uncertainty.

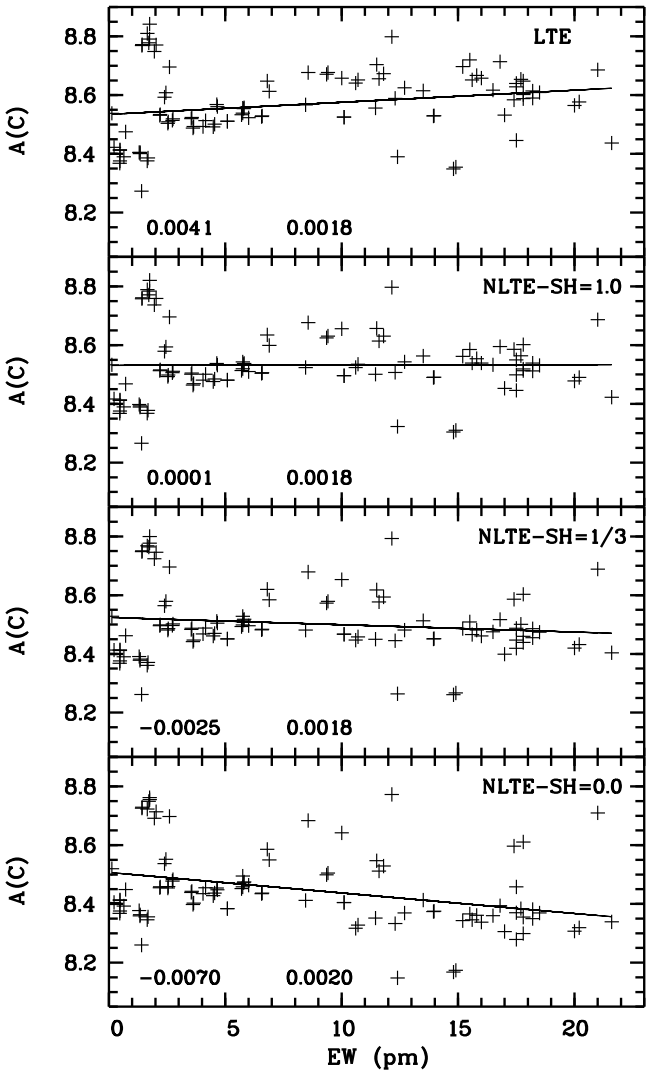

Fig. 6. The carbon abundances as a function of *EW* for the HM model.

There is, however, a clear trend for the 3D-LTE abundances to increase with *EW* (see Fig. 5). The trend is reduced or even reversed after application of the NLTE corrections, depending on the choice of $S_{\rm H}$. As illustrated in Fig. 5, there is a slight negative trend of the 3D-NLTE abundance with *EW* for $S_{\rm H} = 0.0$, and a slightly positive one for $S_{\rm H} = 1/3$. The trend vanishes for a value of $S_{\rm H}$ somewhere in the range $[0, 1/3]$. The corresponding results obtained using the HM model are shown in Fig. 6. This behaviour is similar to what is found with the 3D model, but the slope of the A(C) − *EW* relations is systematically reduced (more negative) in all cases. The results from the HM model suggest that the slope vanished for $S_{\rm H}$ close to 1. The correlation $A(\mathrm{C})_{\rm LTE} - EW$ persists even if we only consider weak lines, indicating that the slope is in fact caused by NLTE effects.

Without available experimental data on cross sections for collisions with neutral hydrogen, one might be tempted to fix the value of $S_{\rm H}$ empirically by requiring a vanishing slope in the A(C) − *EW* plane. Our 3D results would then suggest that $0.0 < S_{\rm H} < 1/3$. However, we prefer to delay this conclusion until a complete 3D-NLTE computation becomes available. In the meantime, since obliged to take a decision, we adopt the intermediate value of $S_{\rm H} = 1/3$, which is the favourite value of the Holweger school.

Our carbon abundances are larger than those derived by Allende Prieto et al. (2002) and Asplund et al. (2005a). The difference is striking if we consider the [CI] line. While the measured *EW*s are similar, we adopt an *EW* that is about 12% smaller than that of Asplund et al. (2005a), owing to the correction for the blending Fe I line. In spite of this, our derived A(C) is 0.11 dex higher than that of Asplund et al. (2005a). This must be ascribed to the difference between the CO5BOLD solar model + Linfor3D and the hydrodynamical simulation and spectral-synthesis code employed by Asplund et al. (2005a). The difference between the models (see Fig. 1 in Caffau et al. 2008) affects both the mean temperature structure and the temperature fluctuations in the region where the [CI] line is formed. Figure 7 shows that the main contribution to the [CI] line absorption comes from the layers between $\log\tau = 0$, to −2 where the differences between the two hydrodynamical simulations are largest. Since the mean temperature gradient is steeper in the 3D model of Asplund et al. (2005a), a lower carbon abundance is needed to reproduce the observed *EW*, in qualitative agreement with the results mentioned above. The same behaviour has been noticed for the [OI] line at 636.3 nm line (see Caffau et al. 2008 and Asplund et al. 2004).

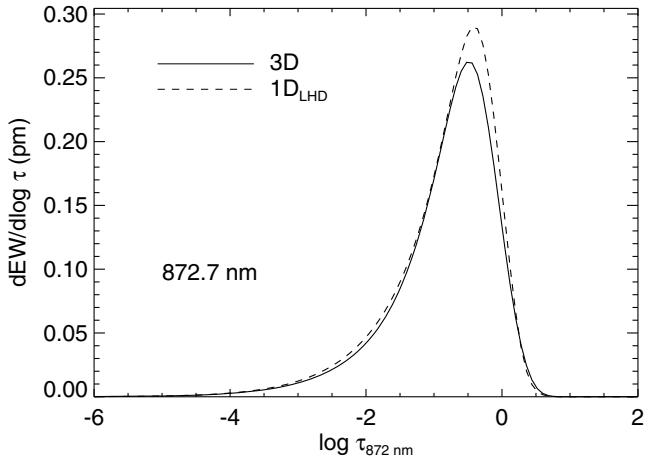

Fig. 7. 3D and 1D$_{LHD}$ *EW* contribution function at disc-centre for the [CI] line a 872.7 nm.

Table 4. Solar abundance of C in the literature.

A(C)	Ref.
8.67 ± 0.10	Lambert (1978)
8.56 ± 0.04	Anders & Grevesse (1989)
8.58 ± 0.13	Stürenburg & Holweger (1990)
8.60 ± 0.05	Grevesse et al. (1991)
8.60 ± 0.10	Bièmont et al. (1993)
8.55	Grevesse et al. (1994)
8.54	Takeda (1994)
8.52 ± 0.06	Grevesse & Sauval (1998)
8.52 ± 0.06	Grevesse et al. (2000)
8.57 ± 0.03	Holweger (2001)
8.592 ± 0108	Holweger (2001)
8.39 ± 0.04	Allende Prieto et al. (2002)
8.39 ± 0.05	Asplund et al. (2005a)
8.39 ± 0.05	Scott et al. (2006)
8.44 ± 0.06	Pinsonneault & Delahaye (2009)
8.39 ± 0.05	Grevesse et al. (2007)
8.43 ± 0.05	Asplund et al. (2009)
8.50 ± 0.06	present work

The situation is similar if we compare the average carbon abundance. From the permitted C I lines, Asplund et al. (2005a) derive $\langle A(\mathrm{C})\rangle = 8.36 \pm 0.03$. This value must be compared with our value of 8.446 ± 0.121, which corresponds to $S_{\mathrm{H}} = 0$, and is consistent with the assumption of Asplund et al. (2005a). Part of the difference stems from our *EW*s, which are generally close to those of Bièmont et al. (1993), hence larger than those of Asplund et al. (2005a). Part of the difference is, however, due to the different hydrodynamical model and/or the different spectrum synthesis code.

In Table 4 the carbon abundance determinations in the past thirty years are listed. The difference of 0.28 dex from the highest to the lowest values cannot be explained by NLTE effects, which, according to our analysis, are about −0.05 dex on average for $S_{\mathrm{H}} = 1/3$. The average of the values in the table is 8.51 with a standard deviation of 0.09.

8. Conclusions

Our recommended value for the solar carbon abundance is $A(\mathrm{C}) = 8.50 \pm 0.06$, corresponding to a weak efficiency of the collisions with neutral hydrogen atoms ($S_{\mathrm{H}} = 1/3$), the favourite value of the Holweger school. The quoted error is the linear sum of a statistical error, 0.02 dex, and a systematic error, 0.04 dex, caused by the uncertainty in the treatment of the hydrogen collisions in the NLTE computation. The statistical error was estimated by dividing the line-to-line scatter, 0.11 dex, by the square root of the 45 independent lines used in the analysis. The value $S_{\mathrm{H}} = 1/3$ was also adopted in our investigations of the solar abundances of oxygen (Caffau et al. 2008) and nitrogen (Caffau et al. 2009b). It is not obvious why the same value of S_{H} should apply to different atoms, or even to different lines of the same atom. It is comforting that the difference between the extreme assumptions about the efficiency of the H collisions ($S_{\mathrm{H}} = 0$ or 1) only amounts to 0.08 dex.

Our preferred value for the solar carbon abundance is very close to the recommendation of Grevesse & Sauval (1998). If we take this carbon abundance, together with $A(\mathrm{N}) = 7.86$ from Caffau et al. (2009b), $A(\mathrm{O}) = 8.76$ from Caffau et al. (2008), and $A(\mathrm{Ne}) = 8.02$ (see Caffau et al. 2009b for an explanation of this choice), we obtain a solar metallicity of $Z = 0.0154$ and $Z/X = 0.0211$. This value is higher than the metallicity recommended by Asplund et al. (2005b) and Grevesse et al. (2007), $Z = 0.0122$, and goes in the direction of reconciling the spectroscopic abundances with the constraints from helioseismology.

That different 3D hydrodynamical simulations provide significantly different results (of the order of 0.1 dex) underlines the need for further development and validation of the hydrodynamical models. Recently, Asplund et al. (2009) have presented results based on a new generation 3D model, which is much closer to the CO^{5}BOLD model than the one used by Asplund et al. (2005a) and which has lead to an upward revision of his carbon, oxygen, and iron abundances. It is likely that any residual difference between this new result and the present analysis can be ascribed to the line selection and to the different treatment of hydrogen collisions in the NLTE computations, although details on the analysis of Asplund et al. (2009) are not yet available. The excellent agreement of our CO^{5}BOLD solar model with the observed centre-to-limb variation, shown in Ludwig et al. (2009), provides strong support for the thermal structure of the model and for the abundances deduced by its application (Caffau et al. 2009a).

Acknowledgements. E.C., H.G.L., and P.B. acknowledge financial support from EU contract MEXT-CT-2004-014265 (CIFIST).

References

Allende Prieto, C., Lambert, D. L., & Asplund, M. 2002, ApJ, 573, L137
Anders, E., & Grevesse, N. 1989, Geochim. Cosmochim. Acta, 53, 197
Asplund, M., Grevesse, N., Sauval, A. J., Allende Prieto, C., & Kiselman, D. 2004, A&A, 417, 751
Asplund, M., Grevesse, N., Sauval, A. J., Allende Prieto, C., & Blomme, R. 2005a, A&A, 431, 693
Asplund, M., Grevesse, N., & Sauval, A. J. 2005b, Cosmic Abundances as Records of Stellar Evolution and Nucleosynthesis, ASP Conf. Ser., 336, 25
Asplund, M., Grevesse, N., Sauval, A. J., & Scott, P. 2009, ARA&A, 47, 481
Ayres, T. R., Plymate, C., & Keller, C. U. 2006, ApJS, 165, 618
Barklem, P. S., Anstee, S. D., & O'Mara, B. J. 1998, PASA, 15, 336
Baschek, B., & Holweger, H. 1967, ZAp, 67, 143
Basu, S., & Antia, H. M. 2008, Phys. Rep., 457, 217
Bièmont, E., Hibbert, A., Godefroid, M., & Vaeck, N. 1993, ApJ, 412, 431
Caffau, E., & Ludwig, H.-G. 2007, A&A, 467, L11
Caffau, E., Ludwig, H.-G., Steffen, M., et al. 2008, A&A, 488, 1031
Caffau, E., Ludwig, H.-G., Steffen, M. 2009a, MmSAI, 80, 3
Caffau, E., Maiorca, E., Bonifacio, P., et al. 2009b, A&A, 498, 877
Castelli, F., & Kurucz, R. L. 2003, in Modelling of Stellar Atmospheres, ed. N. Piskunov et al., Poster A20, IAU Symp., 210 [arXiv:astro-ph/0405087]
Chaplin, W. J., & Basu, S. 2008, Sol. Phys., 251, 53
Delahaye, F., & Pinsonneault, M. H. 2006, ApJ, 649, 529
Delbouille, L., Roland, G., & Neven, L. 1973, Liège: Université de Liège, Institut d'Astrophysique, 1973

Delbouille, L., Roland, G., & Brault, T. 1981, Photometric atlas of the solar spectrum from 1850 to 10 000 cm^{-1}, http://bass2000.obspm.fr/solar_spect.php
Drawin, H. W., 1969, Z. Phys., 225, 483
Farmer, C. B., Norton, R. H., & Geller, M. 1989, NASA Ref. Publ., 1224
Farmer, C. B. 1994, Infrared Sol. Phys., 154, 511
Freytag, B., Steffen, M., & Dorch, B. 2002, Astron. Nachr., 323, 213
Freytag, B., Steffen, M., Wedemeyer-Böhm, S., & Ludwig, H.-G. 2003, CO5BOLD User Manual, http://www.astro.uu.se/~bf/co5bold_main.html
Grevesse, N., Sauval, A. J., Farmer, C. B., & Norton, R. H. 1987, Liege International Astrophysical Colloquia, 27, 111
Grevesse, N., Lambert, D. L., Sauval, A. J., et al. 1991, A&A, 242, 488
Grevesse, N., Sauval, A. J., & Blomme, R. 1994, Infrared Sol. Phys., 154, 539
Grevesse, N., & Sauval, A. J. 1998, Space Sci. Rev., 85, 161
Grevesse, N., Sauval, A., & Murdin, P. 2000, Encyclopedia of Astronomy and Astrophysics
Grevesse, N., Asplund, M., & Sauval, A. J. 2007, Space Sci. Rev., 130, 105
Hibbert, A., Biemont, E., Godefroid, M., & Vaeck, N. 1993, A&AS, 99, 179
Holweger, H. 1967, ZAp, 65, 365
Holweger, H. 2001, Joint SOHO/ACE workshop Solar and Galactic Composition, AIP Conf. Proc., 598, 23
Holweger, H., & Müller, E. A. 1974, Sol. Phys., 39, 19
Kurucz, R. L. 2005a, Mem. Soc. Astron. Ital. Suppl., 8, 189
Lambert, D. L. 1978, MNRAS, 182, 249
Ludwig, H.-G., Caffau, E., Bonifacio, P., et al. 2009, in ed. K. Cunha, M. Spite, & B. Barbuy, IAU Symp., 265
Luo, D., & Pradhan, A. K. 1989, J. Phys. B Atomic Mol. Phys., 22, 3377
Neckel, H., & Labs, D. 1984, Sol. Phys., 90, 205
Neckel, H. 1999, Sol. Phys., 184, 421
Nussbaumer, H., & Storey, P. J. 1984, A&A, 140, 383
Pinsonneault, M. H., & Delahaye, F. 2009, ApJ, 704, 1174
Ralchenko, Y. 2005, Mem. Soc. Astron. Ital. Supp., 8, 96
Ryan, S. G. 1998, A&A, 331, 1051
Scott, P. C., Asplund, M., Grevesse, N., & Sauval, A. J. 2006, A&A, 456, 675
Steenbock, W., & Holweger, H. 1984, A&A, 130, 319
Steffen, M., & Holweger, H. 2002, A&A, 387, 258
Stürenburg, S., & Holweger, H. 1990, A&A, 237, 125
Takeda, Y. 1994, PASJ, 46, 53
Tody, D. 1993, Astronomical Data Analysis Software and Systems II, 52, 173
Wedemeyer, S., Freytag, B., Steffen, M., Ludwig, H.-G., & Holweger, H. 2004, A&A, 414, 1121
Weiss, A. W. 1996, priv. comm. NIST
Wiese, W. L., Fuhr, J. R., & Deters, T. M. 1996, Atomic transition probabilities of carbon, nitrogen, and oxygen: a critical data compilation, ed. W. L. Wiese, J. R. Fuhr, & T. M. Deters (Washington, DC: American Chemical Society), for the National Institute of Standards and Technology (NIST), QC 453, 53
Yang, W. M., & Bi, S. L. 2007, ApJ, 658, L67